ACS Catalysis

Research Article

pubs.acs.org/acscatalysis

Free-Standing Pt–Au Hollow Nanourchins with Enhanced Activity and Stability for Catalytic Methanol Oxidation

Hongjun You, Fangling Zhang, Zhen Liu, and Jixiang Fang*

State Key Laboratory for Mechanical Behavior of Materials, School of Science, Xi'an Jiaotong University, Xianning West Road, Shaan Xi 710049, P.R. China

Supporting Information

ABSTRACT: Controlling the morphology of Pt–Au bimetal nanostructures can provide a great opportunity to increase their catalytic activity on a Pt mass basis and improve their durability at the same time. In this study, we synthesized Pt-on-Au hollow urchinlike nanoparticles (NPs), which present a structure consisting of a monolayer of small Pt NPs uniformly overgrown on an Au hollow nanourchin (HNU). The Pt–Au HNUs demonstrated an ultrahigh density of sharp tips and uniform coating of 2 nm Pt NPs. This well-controlled bimetal nanostructure exhibited a large electrochemical surface area, more than 2 times higher than that of Pt black, and a relatively high electrocatalytic activity toward the methanol oxidation reaction, more than 3 times greater than the Pt black and Pt/C commercial reference catalysts. Simultaneously, the Pt–Au HNUs showed greatly improved durability because of the small Pt NPs on the surface of Pt–Au HNUs which were effectively stabilized by the Au metal support.

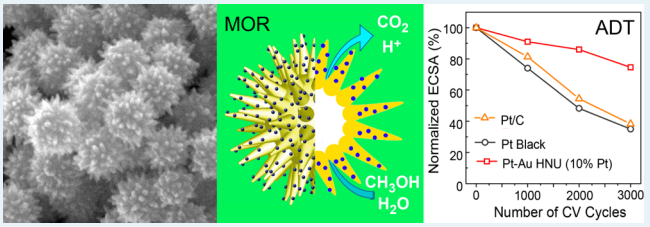

KEYWORDS: *fuel cells, electrochemistry, electrocatalysis, Pt–Au bimetal nanostructure, methanol oxidation reaction*

INTRODUCTION

With the increase of environmental concerns in recent years, there is an urgent demand for new technology that does not rely on fossil fuels. In this context, polymer electrolyte membrane fuel cells (PEMFCs) have been examined as a class of devices to provide clean and sustainable power by directly converting chemical energy stored in fuel molecules into electric energy.[1−3] For PEMFCs, expensive Pt/Pd metals are essential elements to ensure outstanding catalytic properties.[4−6] Improving the activity and durability of catalysts and thus decreasing the usage of Pt/Pd metals is one of the major challenges for widespread applications of fuel cells.[4,7]

To decrease the usage of Pt/Pd metals, nanoparticles (NPs) are expected to be synthesized as small as possible.[8] However, with the size decrease, the specific activity of NPs for methanol oxidation reaction (MOR) or oxygen reduction reaction (ORR) will be decreased gradually. Thus, the maximum mass activity of the current most widely used catalyst appears at 2−3 nm for Pt NPs.[9,10] Cost and supply constraints for large-scale applications require a factor of at least a 4 times increase in catalytic activity per mass for the current Pt NP catalyst.[11] On the other hand, for the small Pt NPs with a size of 2−3 nm, the high surface energy and zero-dimensional structural features will induce Ostwald ripening and Pt atoms dissolution during the voltage cycling, resulting in a significant loss of electrochemical surface area (ECSA) and a fast drop in power output.[12]

One of the typical strategies for improving the mass activity of Pt-based catalysts is the alloying technique or texturing bimetallic nanostructures to incorporate non-Pt metals into the Pt NPs.[4] The bimetallic nanostructures usually include core–shell and Pt-on-M (M: non-Pt metal) structures.[13−17] In these structures, Pt metal is located at the surface, and non-Pt metal is imbedded in the core of the NPs. Thus, not only is the usage of Pt metal obviously decreased but also the activity is greatly enhanced as a result of various contributions such as modulating the transfer of charge, density of electronic states, local coordination environment, as well as lattice stain between Pt and non-Pt metal.[18] Up to now, Pt-on-Au,[19−22] Pt-on-Pd,[23,24] Pt-on-Ru,[25] Pt-on-Co,[26] and Pt-on-Cu[27] heterostructures have been synthesized as electrocatalysts, and improved performance has been observed in these systems. On the other hand, to improve the durability of Pt catalysts against the loss of ECSA, other researchers have developed techniques to construct large NPs with large specific surface area, such as nanowire, hollow, and hierarchical nanostructures.[28−31] This is due to the fact that these nanostructures with larger volume are more stable than small NPs, and they show highly enhanced stability and activity.[30,32−34]

Here, we combined these two typical strategies together and synthesized Pt-on-Au hollow nanourchins (Pt–Au HNUs). In this nanostructure, 2 nm Pt NPs uniformly grew on the surface of Au HNUs. As a support, Au HNUs have both large volume and large specific surface area owing to the hollow interior and ultrahigh density of sharp tips on the surface. The small Pt NPs overgrown on the surface of Pt–Au HNUs were well stabilized

Received: March 24, 2014
Revised: July 15, 2014
Published: July 16, 2014

by the large Au HNUs basis, and thus both electrocatalytic activity and durability were greatly enhanced in the MOR system. At the same time, the large specific surface area of Au HNUs can also greatly decrease the usage of Au metal.

RESULTS AND DISCUSSION

1. Morphology Control of Pt–Au HNUs. The fabrication process of Pt–Au HNUs is illustrated in Figure 1. In this process, Au HNUs were first synthesized through a seed-mediated method, following our previously reported procedures.[35] As shown in Figure 1a, spherical Ag NPs were synthesized and used as seeds to prepare the Au HNUs through a combination process containing the galvanic replacement reaction and chemical growth. Equivalent to the synthesis using Ag or Ag_2O NPs as sacrificial templates to prepare the hollow or porous metal NPs,[30,36,37] the galvanic replacement occurred at the surface of Ag seeds. The produced Au atoms aggregated on the surface of Ag NPs to form small Au NPs. These small Au NPs connected each other to form a shell on the surface. At the same time, the inner Ag atoms diffused to the surface and dissolved into solution after being oxidized into Ag^+ ions during the galvanic replacement reaction. Thus, the hollow structure was formed (Figure 1b) in the center of NPs. As the reaction proceeded, more Au ions were reduced into atom by dopa and grew on the small Au NPs-connected shell. Previous report indicated that the dopa molecules could direct these Au atoms to form a protuberant growth.[38] Thus, on top of each small Au NP, spikelike tips are grown out under the direction of dopa molecules. Finally, plenty of spikelike tips were densely produced on the hollow particle surface. Depending on the shape, these obtained particles were named Au HNUs.

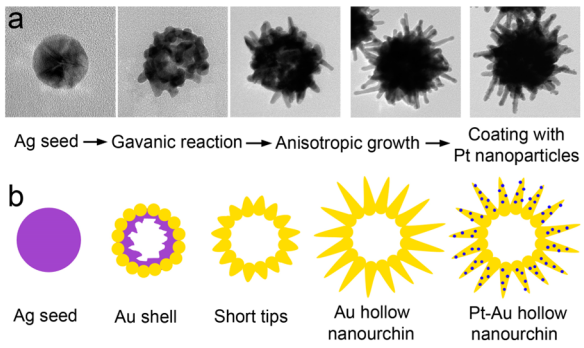

Figure 1. Formation process of Pt–Au HNUs. (a) TEM images of structural evolution from silver seeds to Pt–Au HNUs. (b) Schematic image of particle structure transformation.

Subsequently, small Pt NPs were overgrown on the surface of Au HNUs to form Pt–Au HNUs. In this step, the as-synthesized Au HNUs were dispersed in chloroplatinic acid aqueous solution. Previous study indicated that the reduction of Pt(IV) ions was harder and slower than Pt(II) ions.[39] Thus, in this study, the Pt(IV) ion was used to obtain slow reduction. In this slow reduction system, the Pt ions were preferentially reduced on the surface of Au HNUs than in the solution as a result of the catalytic function of Au metal. In this process, the Pt atoms were slowly and uniformly produced on the surface of Au HNUs. Depending on the Volmer–Weber (V–W) mode,[40] the produced Pt atoms would accumulate and grow into small Pt NPs on the surface of Au HNUs. The overgrown Pt NPs were uniformly distributed on the surface and formed a strong connection with the Au substrate. If the Pt NPs were not produced on the surface of Au HNUs (i.e., while in the solution and following when they were loaded on the surface), they would aggregate and preferentially be deposited in the concaves of Au HNUs. On the other hand, the connection of Pt NPs to Au substrate was also weaker than that of the directly overgrown Pt NPs on the Au surface.

The typical scanning electron microscopy (SEM) images of Au HNUs and Pt–Au HNUs are shown in Figure 2a and b,

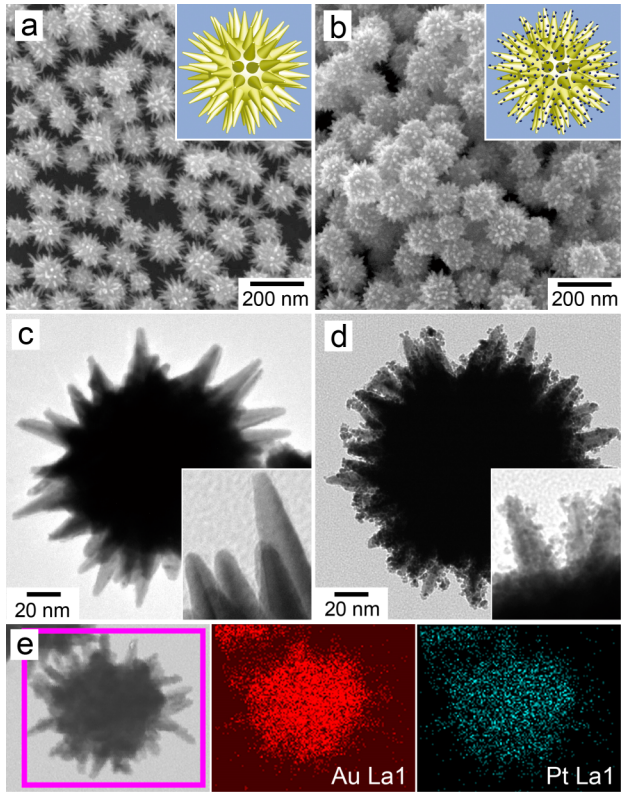

Figure 2. (a,b) SEM images of (a) Au HNUs and (b) Pt–Au HNUs (10% Pt). The insets in (a,b) are the cartoon images of Au HNU and Pt–Au HNU. (c,d) TEM images of (c) Au HNU and (d) Pt–Au HNU (10% Pt). The insets in (c,d) are the corresponding highly magnified TEM images. (e) Elemental analysis of Pt–Au HNU.

respectively. The Au HNUs are uniform in both size and morphology. Their average size is around 150 nm, smaller than the Au NUs reported in previous work.[41,42] At the same time, the current Au HNUs show a higher density of sharper tips (i.e., >100 tips within an individual ~150 nm particle). After being decorated with small Pt NPs, the Pt–Au HNUs keep the similar morphology as before. Only the tips become a little thick. The transmission electron microscopy (TEM) images of Au HNUs and Pt–Au HNUs are shown in Figure 2c and d. The images show that the surface of Au HNUs is densely covered by spike-like tips. The length and diameter of the tips are around 50 and 8 nm, respectively. The specific surface area of current Au HNUs is greatly increased compared with previous reports,[41,42] owing to the hollow structure and densely distributed sharp tips. The TEM image in Figure 2d demonstrates that the surface of Pt–Au HNU is coated by a monolayer of uniform Pt small NPs.

The distributions of the metallic elements in the Pt–Au HNUs were analyzed using the X-ray element mapping and linear scanning. The results in Figure 2e and Figure S1 show

dx.doi.org/10.1021/cs500390s | ACS Catal. 2014, 4, 2829–2835

that the Pt metal element is uniformly distributed on the entire surface of the particle. The amount of Pt metal component in the Pt−Au HNUs was determined using inductively coupled plasma atomic emission spectroscopy (ICP-AES), and the result shows that 10% Pt metal is included in the particle. The Pt mass ratio can be tuned by changing the quantity of Pt precursors in the synthesis. The Pt−Au HNUs with low (5%) and high (15%) Pt mass ratio were obtained by adding 0.4 and 1.2 mL of chloroplatinic acid (H_2PtCl_6, 1 mM), respectively. Figure S2a,b show the SEM images of Pt−Au HNUs with 5% and 15% Pt metal. Their morphologies are similar to the Pt−Au HNU with 10% Pt under SEM images. Under TEM observation (Figure S3), it is found that only small amount of Pt NPs are overgrown on the Pt−Au HNUs with 5% Pt, whereas multiple Pt NPs (more than one layer) are deposited on the Pt−Au HNUs with 15% Pt.

The composition of the Pt−Au HNUs (10% Pt) was further probed by X-ray photoelectron spectroscopy (XPS), and the result is shown in Figure 3. The positions of the XPS spectra

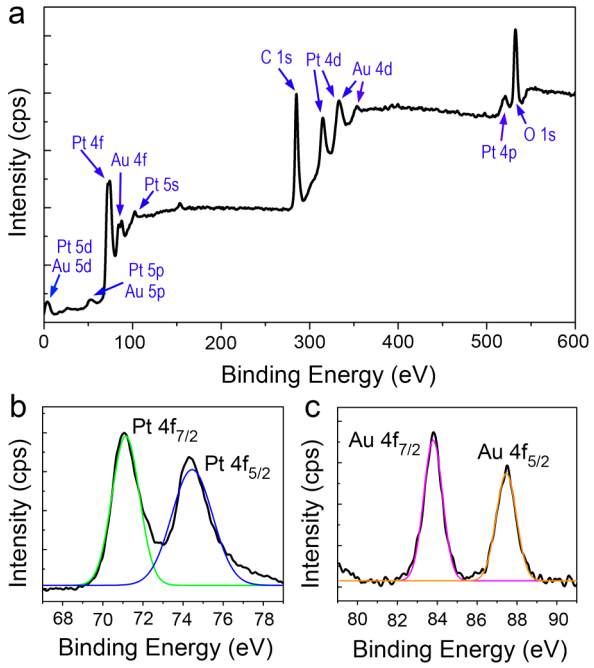

Figure 3. (a) XPS spectra of Pt−Au HNUs (10% Pt), (b) Pt 4f, and (c) Au 4f XPS spectra for Pt−Au HNUs (10% Pt).

peaks (Figure 3a) match with the elements of Pt, Au, C and O. Among these elements, C and O could come from capping agents and surroundings. From the located XPS spectra (Figure 3b,c), it can be observed that the binding energies of Pt 4f (71.0 and 74.4 eV) are shifted to higher values (71.1 and 74.5 eV) and that of Au 4f (84.0 and 87.7 eV) are shifted to lower values (83.8 and 87.5 eV), compared to the standard data of Pt^0 and Au^0 species. The increase in the binding energy of Pt 4f and the decrease in Au 4f suggest that the electron transfer from Pt to Au in the bimetallic Pt−Au HNUs could be occurred, which can be related to the perturbed electronic interaction between Pt and Au atomic orbit. The increased binding energy of Pt atoms may contribute to a potential increase in the durability of Pt−Au bimetallic electro-catalyst.

The crystal structures of Au HNUs and Pt−Au HNUs were characterized by means of high-resolution TEM (HR-TEM). Figure 4a shows a HR-TEM image of a single spike-like Au tip,

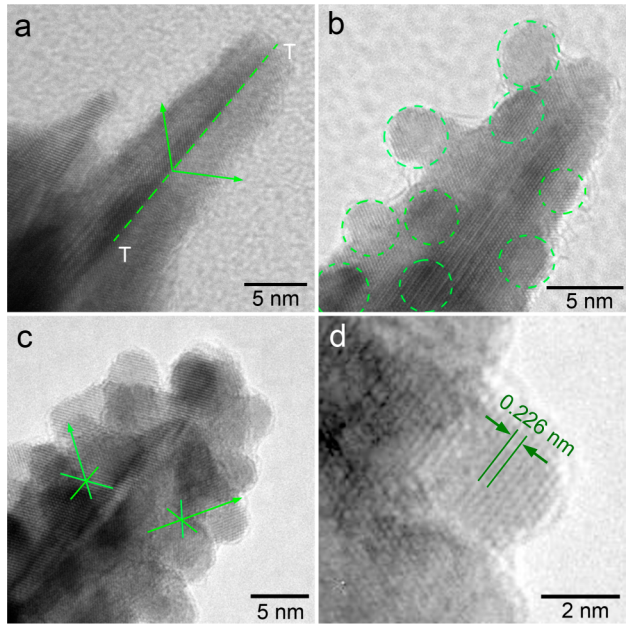

Figure 4. HR-TEM images of (a) Au HNUs and (b−d) Pt−Au HNUs. The ratios of Pt metal are 10% and 15% in (b) and (c), respectively. (d) Magnified image from (c).

which clearly displays a twin plane in the center. The twin plane indicates that the formation of the spike-like tips was enabled by a twin plane-induced anisotropic growth.[4] Figure 4b−d show the HR-TEM images of the tips for the Pt−Au HNUs. Same as the TEM image, the HR-TEM images also show that a monolayer consisting of uniform 2 nm spherical Pt NPs are overgrown on the surface of Pt−Au HNUs (10% Pt) (Figure 4b). However, in the case of 15% Pt, more than one layer of Pt NPs are overgrown on the surface (Figure 4c). The HR-TEM images also show that continuous lattice fringes are shared between Au tips and Pt NPs. The lattice mismatch between Pt and Au is 3.9%, indicating that the Pt NPs can be epitaxially overgrown on the Au tips through the Volmer−Weber (V−W) mode.[40] The lattice space of the Pt NPs (Figure 4d) is 0.226 nm, which matches well with Pt {111} planes *d*-spacing (0.226 nm).

2. Electrocatalytic Properties of Pt−Au HNUs. The electrocatalytic properties of the as-prepared free-standing Pt−Au HNUs with different Pt ratios (5%, 10%, and 15% Pt) were evaluated. Two kinds of commercial Pt-based catalysts (i.e., Pt black (Alfa Aesar, fuel cell grade) and Pt/C (40 wt % Pt, JM)) were also tested for comparison. First, the cyclic voltammetry (CV) curves of five catalysts were recorded at room temperature in argon-purged 0.1 M $HClO_4$ solutions at a sweep rate of 50 mV/s. As shown in Figure 5a, the CV curves exhibited two distinctive potential regions associated with the H_{upd} ($H^+ + e^- = H_{upd}$) adsorption/desorption between 0.0 and 0.37 V and the formation of OH_{ad} layer ($2H_2O = OH_{ad} + H_3O^+ + e^-$) in the range of 0.6−1.2 V. The ECSAs of five catalysts were calculated and shown in Figure 5b by measuring the charge collected in the H_{upd} adsorption/desorption region after double-layer correction and assuming a value of 210 $\mu C/cm^2$ for the adsorption of a hydrogen monolayer.[43] The specific ECSAs (the ECSA per unit weight of Pt metal) of Pt−Au HNUs with 5% and 10% Pt are 41.8 and 36.3 m^2/g_{Pt}, which are more than 2 times higher than that of Pt black (18.0 m^2/g_{Pt}) and close to that of Pt/C (35.8 m^2/g_{Pt}). Under the free-

dx.doi.org/10.1021/cs500390s | ACS Catal. 2014, 4, 2829−2835

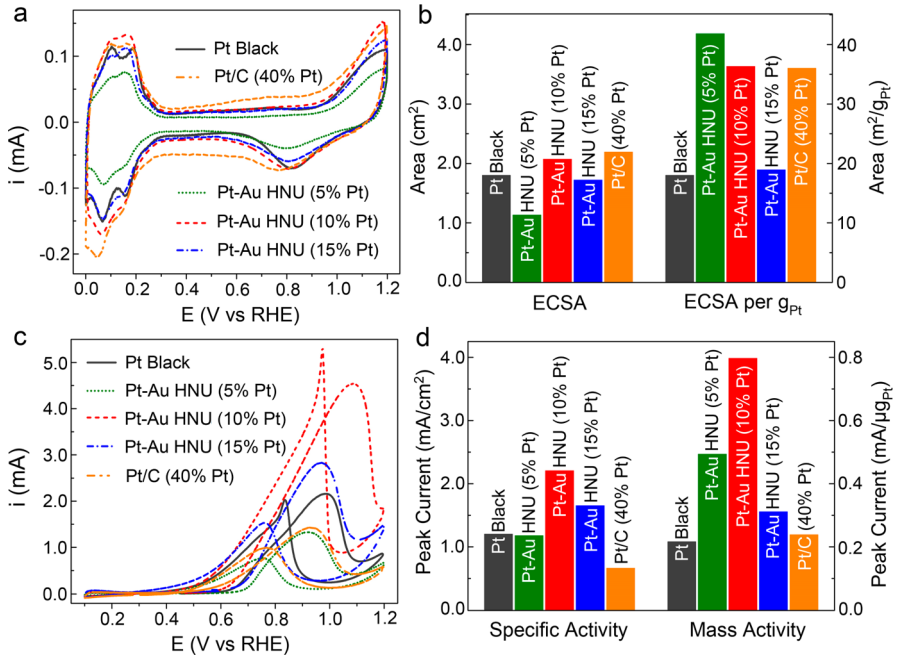

Figure 5. (a) CV curves obtained for the Pt black, Pt/C, and Pt−Au HNUs in argon-saturated 0.1 M $HClO_4$ solution at 50 mV/s. (b) ECSAs and ECSAs per Pt gram for five catalysts. (c) Methanol oxidation reaction catalyzed by the five catalysts in argon-saturated 0.1 M $HClO_4$ + 0.5 M CH_3OH solution at 50 mV/s. (d) Specific activity and mass activity of the five catalysts.

standing situation, the extensive agglomeration was formed in the Pt black catalyst. However, for the Pt−Au HNUs with 5% and 10% Pt, the Pt NPs were fastened on the surface of Au HNUs. Thus, the aggregation effect may be prevented. In the Pt−Au HNUs with 15% Pt, more than one layer Pt NPs were overgrown on the surface, thus the specific ECSA was greatly decreased.

The electrocatalytic property of Pt−Au HNUs for MOR was tested and compared with the Pt black and Pt/C catalysts in an argon-purged 0.1 M $HClO_4$ + 0.5 M CH_4O solution at a scan rate of 50 mV/s. The CV curves of MOR (Figure 5c) show little difference in the shape among the Pt−Au HNUs, Pt black, and Pt/C catalysts, suggesting that the reaction pathway should be similar.[44] The specific activities of five catalysts at peak current for MOR were calculated and shown in Figure 5d. The Pt−Au HNUs with 10% Pt shows the highest catalytic activity. In light of the normalized peak current against the ECSA, the Pt−Au HNUs with 10% Pt have a specific activity of 2.25 mA/cm^2 that is 1.9 times that of Pt black and 3.4 times that of Pt/C. In a previous report, the specific activities of Pt−Au nanoporous leaf and surface composition tuned Pt−Au NPs (68% Pt_{surf}) for MOR are 1.7 and 2.1 mA/cm^2 that are 1.8 and 2.4 times that of Pt/C, respectively, less than the 3.4 times in this work.[45,46]

The Pt−Au HNUs with 10% Pt also show the highest mass activity for MOR, reaching 0.80 mA/μg_{Pt}, which is 3.7 times that of Pt black and 3.3 times that of Pt/C. Different with the agglomeration of Pt NPs in the Pt black, the Pt NPs are well dispersed and uniformly supported on the surface of the Au HNUs, thus contributing to a high mass activity. On the other hand, different with the carbon support in the Pt/C, the Au support in the Pt−Au HNUs may improve the Pt activity due to some factors such as the modulating the transfer of charge, the density of electronic states, the local coordination environment, as well as the lattice stain between Pt and Au metal (as shown by the XPS and HR-TEM results in Figures 3 and 4).[18] In a previous report using materials such as Pt−Au nanosponges, Pt−Au NPs on grapheme, and nanoporous bimetallic Pt−Au alloy composite, the mass activities are 0.347, 0.394, and 0.348 mA/μg_{Pt}, respectively, which are 1.6 to 2.0 times that of Pt/C, less than the 3.3 times in this work.[47−49]

The catalytic result of Pt−Au HNUs with different Pt ratio shows that the amount of Pt NPs on the surface of Pt−Au HNUs has an important effect on the catalytic property. As shown in Figure 5d, the optimum activity occurs when 10% Pt is loaded on the Pt−Au HNUs surface. This result is similar to the previous report for Pt−Au alloy NPs where the optimal MOR activity appears when the Pt composition on the NP surface is ∼70 atom %.[46] In that study, if all of Au metal is embedded in the center of particle and the surface is covered only by Pt metal, like the core−shell structure, the improvement of Au metal for catalytic activity will be inhibited. The exposed Au atoms have a more obvious improvement for the catalytic property of Pt metal in the Pt−Au bimetallic nanostructure. On the contrary, too much exposed Au metal will decrease the catalytic property of Pt metal. From the reported composition ratio on the surface of Pt−Au alloy NPs, it can be deduced that the optimal ratio between the exposed Au and Pt areas on the surface is around 1:3.[46] In our Pt−Au HNUs with 15% Pt, more than one layer of Pt NPs was overgrown on the surface, and the Au metal was imbedded in the center by the Pt NPs. Thus, the catalytic property became worse compared with the Pt−Au HNUs with 10% Pt. On the contrary, a reduced amount of Pt NPs on the surface in the Pt−Au HNUs with 5% Pt also would decrease the catalytic activity.

The surface poisoning rates of five catalysts were evaluated using chronoamperometry at a constant potential of 0.65 V. As shown in Figure S4, the polarization currents for all the catalysts decrease rapidly because of the formation of intermediate species during the MOR process.[46−48] In contrast, the Pt−Au HNUs with 10% Pt show much slower current density decay over time, indicating a better tolerance to the

dx.doi.org/10.1021/cs500390s | ACS Catal. 2014, 4, 2829−2835

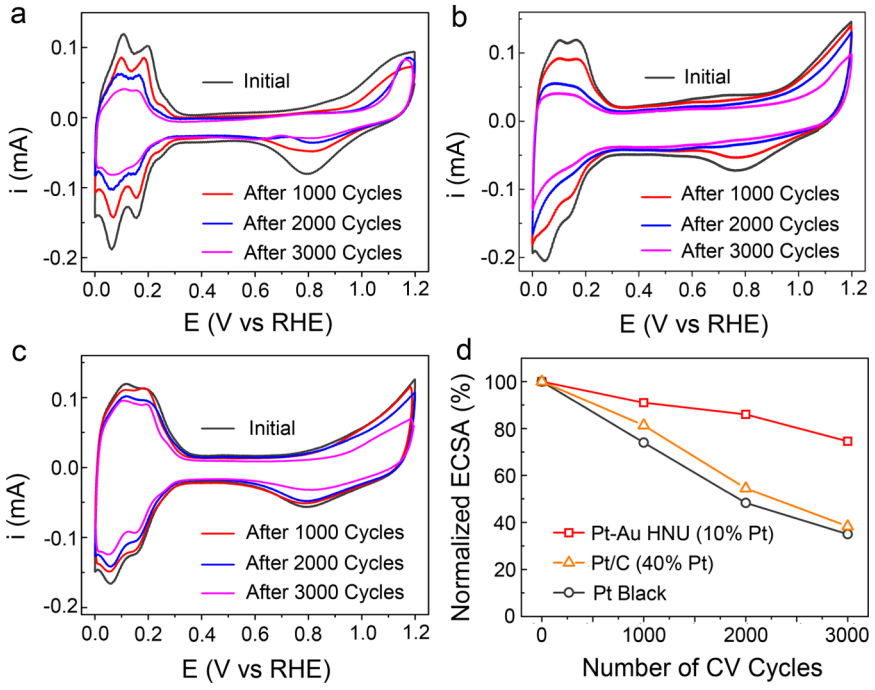

Figure 6. Comparison of electrochemical durability for the Pt black, Pt/C, and Pt–Au HNU (10% Pt) catalysts. (a,b) CV curves obtained in argon-saturated 0.1 M $HClO_4$ solution at 50 mV/s for (a) Pt black, (b) Pt/C, and (c) Pt–Au HNU before and after different cycles of ADT. In the ADT, the potential cycles were scanned from 0.6 to 1.1 V (vs RHE) in an O_2-saturated 0.1 M $HClO_4$ solution at room temperature. (d) ECSA loss of Pt black, Pt/C, and Pt–Au HNU with the increase of CV cycles.

catalyst poisoning intermediates. The anode catalytic properties of Pt–Au HNUs with 10% Pt for formic acid oxidation reaction (FAOR) and ethanol oxidation reaction (EOR) were also tested and compared with the Pt black catalyst. As shown in Figure S5 and S6, the results demonstrate that the incorporation of Au with Pt can enhance not only the electrocatalytic activity for MOR but also that of FAOR and EOR.

The durability of catalyst also has been recognized as one of the most important issues to be addressed before the commercialization of PEMFCs.[3,13] Thus, the stability of Pt–Au HNUs with 10% Pt was further evaluated in an accelerated durability test (ADT) by applying linear potential sweeps between 0.6 and 1.1 V at 50 mV/s in O_2-saturated 0.1 M $HClO_4$ solution at room temperature. For comparison, the Pt black and Pt/C catalysts were also studied under identical conditions. Figure 6a–c show the CV curves of Pt–Au HNUs (10% Pt), Pt black, and Pt/C catalysts before and after 3000 ADT cycles. The current densities in the hydrogen adsorption/desorption potential regions (0–0.37 V) for the Pt black and Pt/C catalysts drops dramatically with the increase of CV cycles (Figure 6a,b). In contrast, the Pt–Au HNUs (10% Pt) exhibit only a slight drop for the current densities in the same potential region (Figure 6c). The loss of ECSA with the increase of CV cycles is plotted in Figure 6d. After 1000, 2000, and 3000 ADT cycles, the ECSA of Pt–Au HNUs (10% Pt) only decreases 9%, 14%, and 25%, respectively. The decrease rate does not change significantly among the entire 3000 cycles test. However, the ECSA loss for the Pt black catalyst is 27%, 52%, and 65% after 1000, 2000, and 3000 ADT cycles, respectively. For the Pt/C catalyst, the decrease rate is very near to the Pt black catalyst. For the Pt black and Pt/C catalysts, the loss rate of ECSA is quicker at the first stage than that at the later stage. As reported in previous work, the Pt NPs would grow up and aggregate during the durability tests owing to the Ostwald ripening.[29] The aggregation and coalescence of Pt NPs in the Pt black and Pt/C catalysts induced the decrease of specific surface area. Concomitant with the size increase, the Pt NPs became stable. Thus, the loss rate of ECSA turned slower at the later stage. Compared with the Pt black and Pt/C catalysts, the process of Ostwald ripening happened much slower in the Pt–Au HNU catalyst.

CONCLUSIONS

In summary, a well-designed bimetallic nanostructure, Pt–Au HNU, was synthesized using a simple method. This new kind of Pt–Au nanostructure has the following advantages as electrocatalyst: (1) The Au HNUs served as support demonstrate high density of sharp tips on the surface (more than 100 tips within individual 150 nm particle) and hollow interior. Thus, the Au HNUs support is more stable than small Au NPs and, at the same time, keeps large specific surface area. As small as 2 nm Pt NPs are overgrown on the surface of Au HNUs and become very stable due to the stabilization of large Au support. The Au HNUs support not only enhances the electocatalytic activity but also greatly improves the durability of Pt NPs, which is crucial for the PEMFC applications. After 3000 ADT cycles, the ECSA loss of Pt–Au HNUs is 14%, only a quarter of that of Pt black and Pt/C catalysts. (2) In the Pt–Au HNUs, the Pt metal only locates on the surface and the amount of Pt NPs on the surface can be controlled in synthesis. This situation is different with the conventional PtAu alloy catalyst where part of Pt metal is imbedded in the center of alloy particle and has no direct catalytic function. However, with tuning the amount of Pt NPs on the surface, the optimal Pt–Au HNUs with highest catalytic activity can be obtained. The Pt–Au HNUs with 10% Pt have 3.7 times higher mass activity than that of Pt black for MOR and 3.3 times than that

dx.doi.org/10.1021/cs500390s | ACS Catal. 2014, 4, 2829–2835

of Pt/C. (3) The Pt−Au HNUs can be used as free-standing catalysts which avoid the corrosion of carbon support existed in the conventional carbon supported catalysts during the electrochemical reaction. Uniform 2 nm Pt NPs overgrow on the surface of Au HNUs and share the same crystalline directions with the Au substrate, forming strong interaction with Au support. Different with the free-standing Pt black catalyst, the aggregation and coalescence of Pt NPs on the Pt−Au HNUs are effectively prevented. Thus, high stability and greatly enhanced activity are both obtained in the Pt−Au HNUs.

EXPERIMENTAL SECTION

Materials. Trisodium citrate dehydrate ($Na_3C_6H_5O_7{\cdot}2H_2O$) 99+ %, silver nitrate ($AgNO_3$) ≥90%, gold(III) chloride hydrate ($HAuCl_4{\cdot}4H_2O$) 99.999%, dopa (3,4-dihydroxyphenylalanine) 98%, chloroplatinic acid hexahydrate ($H_2PtCl_6{\cdot}6H_2O$) 99.995%, and L-ascorbic acid 99.7% were all used without further purification. Deionized water (Millipore) with a resistivity of 18.2 MΩ-cm was used in all preparations.

Synthesis of Pt−Au HNUs. In this process, Au HNUs were first prepared using previously reported method.[35] The details are shown in the Supporting Information. Following, Pt NPs were overgrown on the obtained Au HNUs. In a typical synthesis, 3 mL of the as-prepared Au HNUs was added to a 25 mL glass vial containing 5.8 mL DI water. Then, 0.8 mL chloroplatinic acid (H_2PtCl_6, 1 mM) was injected. After magnetic stirring (100 rpm) for 1 h, 0.4 mL of L-ascorbic acid (100 mM) was fed into the vial with vigorous stirring (400 rpm) to make the solution quickly mixed. After 1 min, the spin rate was slowed down to 100 rpm and kept for 10 min. After that, the vial was put into a water bath of 50 °C for 10 h. Finally, the black product was centrifuged (6000 rpm) and washed 10 times using DI water. The Pt−Au HNUs with different amount of Pt have been synthesized by changing the feeding of the Pt precursor from 0.4 to 1.2 mL.

Characterization. The SEM images were taken on a JSM-7000F field-emission scanning electron microscopy at an accelerating voltage of 10 kV. The TEM and HR-TEM images were acquired on a JEM- 2100 microscope at an accelerating voltage of 200 kV. The elemental maps were carried out using the high-angle annular dark-field (HAADF) mode on a JEOL (TEM-2100F) microscope at an accelerating voltage of 200 kV. The XPS measurement was carried out using a VG Scientific (ESCALAB 250) photoelectron spectrometer. The X-ray source was Al Kα with 1486.6 eV operating at 150 kV and 150 W. The composition of Pt−Au HNUs was determined through inductively coupled plasma atomic emission spectrometry (ICP-AES 5300).

Measurement of Electrocatalytic Properties. The electrochemical measurement was performed on a VersaSTAT 3 electrochemical working station using a three-electrode cell. The working electrode was a glassy-carbon rotating disk electrode (GCE, 5 mm in diameter). A 1 cm^2 platinum foil was used as the counter electrode, and a double junction Ag/AgCl electrode was used as the reference. All potentials in this study were transformed to refer to that of reversible hydrogen electrode (RHE). The DI water suspensions of the as-synthesized Pt−Au HNUs (20 μL) were dripped onto the surface of the GCE and dried at room temperature. After evaporation of the water, 10 μL Nafion solution (0.05 wt %, diluted from 5 wt % Nafion, Ion Power, Inc.) was covered on the surface and dried in a stream of air to attach the catalyst particles on to the GCE. All of the measurements were conducted at room temperature (25 °C).

ASSOCIATED CONTENT

Supporting Information

Supplementary and additional information as noted in the text. This material is available free of charge via the Internet at http://pubs.acs.org.

AUTHOR INFORMATION

Corresponding Author

*E-mail: jxfang@mail.xjtu.edu.cn.

Notes

The authors declare no competing financial interest.

ACKNOWLEDGMENTS

This work was supported by National Natural Science Foundation of China (nos. 51201122 and 51171139), Doctoral program of higher education of China (nos. 20120201120049, 20130201110032 and 20110201120039) and the Fundamental Research Funds for the Central Universities (nos. 08142023, 08143077 and xkjc2014004). J.-X.F. was supported by Scientific New Star Program in Shaanxi Province (no. 2012KJXX-03).

REFERENCES

(1) Gasteiger, H. A.; Markovic, N. M. *Science* **2009**, *324*, 48−49.
(2) Yang, H.; Yin, Y. D. *ChemSusChem* **2013**, *6*, 1781−1783.
(3) Borup, R.; Meyers, J.; Pivovar, B.; Kim, Y.; Mukundan, R.; Garland, N.; Myers, D.; Wilson, M.; Garzon, F.; Wood, D.; Zelenay, P.; More, K.; Stroh, K.; Zawodzinski, T.; Boncella, J.; McGrath, J.; Inaba, M.; Miyatake, K.; Hori, M.; Ota, K.; Ogumi, Z.; Miyata, S.; Nishikata, A.; Siroma, Z.; Uchimoto, Y.; Yasuda, K.; Kimijima, K.; Iwashita, N. *Chem. Rev.* **2007**, *107*, 3904−3951.
(4) H. You, H. J.; Yang, S. C.; Ding, B. J.; Yang, H. *Chem. Soc. Rev.* **2013**, *42*, 2880−2904.
(5) Wang, C.; Daimon, H.; Onodera, T.; Koda, T.; Sun, S. H. *Angew. Chem., Int. Ed.* **2008**, *47*, 3588−3591.
(6) Zhang, H.; Jin, M. S.; Xia, Y. N. *Chem. Soc. Rev.* **2012**, *41*, 8035−8049.
(7) Bing, Y. H.; Liu, H. S.; Zhang, L.; Ghosh, D.; Zhang, J. J. *Chem. Soc. Rev.* **2010**, *39*, 2184−2202.
(8) Sun, Y.; Zhuang, L.; Lu, J.; Hong, X.; Liu, P. *J. Am. Chem. Soc.* **2007**, *129*, 15465−15467.
(9) Mukerjee, S.; McBreen, J. *J. Electroanal. Chem.* **1998**, *448*, 163−171.
(10) Kinoshita, K. *J. Electrochem. Soc.* **1990**, *137*, 845−848.
(11) Gasteiger, H. A.; Kocha, S. S.; Sompalli, B.; Wagner, F. T. *Appl. Catal., B* **2005**, *56*, 9−35.
(12) Yu, X. W.; Ye, S. Y. *J. Power Sources* **2007**, *172*, 133−144.
(13) Zhang, J.; Sasaki, K.; Sutter, E.; Adzic, R. R. *Science* **2007**, *315*, 220−222.
(14) Kim, Y.; Hong, J. W.; Lee, Y. W.; Kim, M.; Kim, D.; Yun, W. S.; Han, S. W. *Angew. Chem., Int. Ed.* **2010**, *49*, 10197−10201.
(15) Kristian, N.; Yan, Y. S.; Wang, X. *Chem. Commun.* **2008**, 353−355.
(16) Yamauchi, Y.; Tonegawa, A.; Komatsu, M.; Wang, H. J.; Wang, L.; Nemoto, Y.; Suzuki, N.; Kuroda, K. *J. Am. Chem. Soc.* **2012**, *134*, 5100−5109.
(17) Wang, L.; Nemoto, Y.; Yamauchi, Y. *J. Am. Chem. Soc.* **2011**, *133*, 9674−9677.
(18) Gu, J.; Zhang, Y. W.; Tao, F. *Chem. Soc. Rev.* **2012**, *41*, 8050−8065.
(19) Yeo, K. M.; Choi, S.; Anisur, R. M.; Kim, J.; Lee, I. S. *Angew. Chem., Int. Ed.* **2011**, *50*, 745−748.
(20) Ye, F.; Liu, H.; Hu, W.; Zhong, J.; Chen, Y.; Cao, H.; Yang, J. *Dalton Trans.* **2012**, *41*, 2898−2903.

(21) Guo, S.; Li, J.; Dong, S.; Wang, E. *J. Phys. Chem. C* **2010**, *114*, 15337−15342.
(22) Lim, S. I.; Varon, M.; Ojea-Jimenez, I.; Arbiol, J.; Puntes, V. *J. Mater. Chem.* **2011**, *21*, 11518−11523.
(23) Lim, B.; Jiang, M.; Camargo, P. H. C.; Cho, E. C.; Tao, J.; Lu, X.; Zhu, Y.; Xia, Y. *Science* **2009**, *324*, 1302−1305.
(24) Peng, Z.; Yang, H. *J. Am. Chem. Soc.* **2009**, *131*, 7542−7543.
(25) Lu, Y.; Chen, W. *Chem. Commun.* **2011**, *47*, 2541−2543.
(26) Tang, S.; Vongehr, S.; Zheng, Z.; Meng, X. *J. Colloid Interface Sci.* **2010**, *351*, 217−224.
(27) Taylor, E.; Chen, S.; Tao, J.; Wu, L.; Zhu, Y.; Chen, J. *ChemSusChem* **2013**, *6*, 1863−1867.
(28) Peng, Z.; You, H.; Wu, J.; Yang, H. *Nano Lett.* **2010**, *10*, 1492−1496.
(29) Liang, H.-W.; Cao, X.; Zhou, F.; Cui, C.-H.; Zhang, W.-J.; Yu, S.-H. *Adv. Mater.* **2011**, *23*, 1467−1471.
(30) Li, T.; You, H. J.; Xu, M. W.; Song, X. P.; Fang, J. X. *ACS Appl. Mater. Interfaces* **2012**, *4*, 6941−6947.
(31) Alia, S. M.; Larsen, B. A.; Pylypenko, S.; Cullen, D. A.; Diercks, D. R.; Neyerlin, K. C.; Kocha, S. S.; Pivovar, B. S. *ACS Catal.* **2014**, *4*, 1114−1119.
(32) Sun, S. H.; Jaouen, F.; Dodelet, J. P. *Adv. Mater.* **2008**, *20*, 3900−3904.
(33) Zhou, H. J.; Zhou, W. P.; Adzic, R. R.; Wong, S. S. *J. Phys. Chem. C* **2009**, *113*, 5460−5466.
(34) Chen, Z. W.; Waje, M.; Li, W. Z.; Yan, Y. S. *Angew. Chem., Int. Ed.* **2007**, *46*, 4060−4063.
(35) Liu, Z.; Yang, Z.; Peng, B.; Cao, C.; Zhang, C.; You, H.; Xiong, Q.; Li, Z.; Fang, J. *Adv. Mater.* **2014**, *26*, 2431−2439.
(36) Yang, Z.; Zhang, L.; You, H.; Li, Z.; Fang, J. *Part. Part. Syst. Charact.* **2014**, *31*, 390−397.
(37) Zhuang, L. N.; Wang, W. J.; Hong, F.; Yang, S. C.; You, H. J.; Fang, J. X.; Ding, B. J. *J. Solid State Chem.* **2012**, *191*, 239−245.
(38) Liu, Z.; Zhang, F.; Yang, Z.; You, H.; Tian, C.; Li, Z.; Fang, J. *J. Mater. Chem. C* **2013**, *1*, 5567−5576.
(39) Tsung, C. K.; Kuhn, J. N.; Huang, W. Y.; Aliaga, C.; Hung, L. I.; Somorjai, G. A.; Yang, P. D. *J. Am. Chem. Soc.* **2009**, *131*, 5816−5822.
(40) Fan, F. R.; Liu, D. Y.; Wu, Y. F.; Duan, S.; Xie, Z. X.; Jiang, Z. Y.; Tian, Z. Q. *J. Am. Chem. Soc.* **2008**, *130*, 6949−6951.
(41) Fang, J. X.; Du, S. Y.; Lebedkin, S.; Li, Z. Y.; Kruk, R.; Kappes, M.; Hahn, H. *Nano Lett.* **2010**, *10*, 5006−5013.
(42) You, H. J.; Ji, Y. T.; Wang, L.; Yang, S. C.; Yang, Z. M.; Fang, J. X.; Song, X. P.; Ding, B. J. *J. Mater. Chem.* **2012**, *22*, 1998−2006.
(43) Schmidt, T. J.; Gasteiger, H. A.; Stab, G. D.; Urban, P. M.; Kolb, D. M.; Behm, R. J. *J. Electrochem. Soc.* **1998**, *145*, 2354−2358.
(44) Franceschini, E. A.; Planes, G. A.; Williams, F. J.; Soler-Illia, G.; Corti, H. R. *J. Power Sources* **2011**, *196*, 1723−1729.
(45) Ge, X. B.; Wang, R. Y.; Liu, P. P.; Ding, Y. *Chem. Mater.* **2007**, *19*, 5827−5829.
(46) Suntivich, J.; Xu, Z. C.; Carlton, C. E.; Kim, J.; Han, B. H.; Lee, S. W.; Bonnet, N.; Marzari, N.; Allard, L. F.; Gasteiger, H. A.; Hamad-Schifferli, K.; Shao-Horn, Y. *J. Am. Chem. Soc.* **2013**, *135*, 7985−7991.
(47) Lin, Z. H.; Shih, Z. Y.; Tsai, H. Y.; Chang, H. T. *Green Chem.* **2011**, *13*, 1029−1035.
(48) Hu, Y. J.; Zhang, H.; Wu, P.; Zhou, B.; Cai, C. X. *Phys. Chem. Chem. Phys.* **2011**, *13*, 4083−4094.
(49) Zhang, Z. H.; Wang, Y.; Wang, X. G. *Nanoscale* **2011**, *3*, 1663−1674.
(50) Hsin, Y. L.; Hwang, K. C.; Yeh, C. T. *J. Am. Chem. Soc.* **2007**, *129*, 9999−10010.
(51) Iwasita, T. *Electrochim. Acta* **2002**, *47*, 3663−3674.
(52) Jiang, L. H.; Sun, G. Q.; Zhao, X. S.; Zhou, Z. H.; Yan, S. Y.; Tang, S. H.; Wang, G. X.; Zhou, B.; Xin, Q. *Electrochim. Acta* **2005**, *50*, 2371−2376.